

## Article

# An Integrated Approach for Investigating the Salinity Evolution in a Mediterranean Coastal Karst Aquifer

Eleonora Frollini <sup>1</sup>, Daniele Parrone <sup>1,\*</sup>, Stefano Ghergo <sup>1</sup>, Rita Masciale <sup>2</sup>, Giuseppe Passarella <sup>2</sup>, Maddalena Pennisi <sup>3</sup>, Matteo Salvadori <sup>3</sup> and Elisabetta Preziosi <sup>1</sup>

<sup>1</sup> Water Research Institute, National Research Council (IRSA-CNR), 00015 Monterotondo (Rome), Italy; eleonora.frollini@irsa.cnr.it (E.F.); stefano.ghergo@irsa.cnr.it (S.G.); elisabetta.preziosi@irsa.cnr.it (E.P.)

<sup>2</sup> Water Research Institute, National Research Council (IRSA-CNR), 70132 Bari, Italy; rita.masciale@ba.irsa.cnr.it (R.M.); giuseppe.passarella@ba.irsa.cnr.it (G.P.)

<sup>3</sup> Institute of Geosciences and Earth Resources, National Research Council (IGG-CNR), 56124 Pisa, Italy; m.pennisi@igg.cnr.it (M.P.); salvadorimatteo@gmail.com (M.S.)

\* Correspondence: daniele.parrone@irsa.cnr.it

**Abstract:** Coastal areas are characterized by considerable demographic pressure that generally leads to groundwater overexploitation. In the Mediterranean region, this situation is exacerbated by a recharge reduction enhanced by climate change. The consequence is water table drawdown that alters the freshwater/seawater interface facilitating seawater intrusion. However, the groundwater salinity may also be affected by other natural/anthropogenic sources. In this paper, water quality data gathered at 47 private and public wells in a coastal karst aquifer in Apulia (southern Italy), were interpreted by applying disparate methods to reveal the different sources of groundwater salinity. Chemical characterization, multivariate statistical analysis, and mixing calculations supplied the groundwater salinization degree. Characteristic ion ratios, strontium isotope ( $^{87}\text{Sr}/^{86}\text{Sr}$ ), and pure mixing modelling identified the current seawater intrusion as a main salinity source, also highlighting the contribution of water–rock interaction to groundwater composition and excluding influence from Cretaceous paleo-seawater. Only the combined approach of all the methodologies allowed a clear identification of the main sources of salinization, excluding other less probable ones (e.g., paleo-seawater). The proposed approach enables effective investigation of processes governing salinity changes in coastal aquifers, to support more informed management.

**Keywords:** groundwater/seawater mixing phenomena; water-rock interaction; geochemical modelling; characteristic ion ratios; strontium isotope ratio; Apulia



**Citation:** Frollini, E.; Parrone, D.; Ghergo, S.; Masciale, R.; Passarella, G.; Pennisi, M.; Salvadori, M.; Preziosi, E. An Integrated Approach for Investigating the Salinity Evolution in a Mediterranean Coastal Karst Aquifer. *Water* **2022**, *14*, 1725. <https://doi.org/10.3390/w14111725>

Academic Editor: Pankaj Kumar

Received: 29 April 2022

Accepted: 25 May 2022

Published: 27 May 2022

**Publisher's Note:** MDPI stays neutral with regard to jurisdictional claims in published maps and institutional affiliations.



**Copyright:** © 2022 by the authors. Licensee MDPI, Basel, Switzerland. This article is an open access article distributed under the terms and conditions of the Creative Commons Attribution (CC BY) license (<https://creativecommons.org/licenses/by/4.0/>).

## 1. Introduction

Coastal areas, also owing to their mild microclimate, support 60–70% of the human population and are characterized by a large concentration of human activities, especially agriculture [1,2]. In the Mediterranean region, the density of inhabitants in coastal areas can reach up to 1300 in/km<sup>2</sup> [3]. This considerable demographic pressure in coastal areas, which increases during the touristic seasons, results in a remarkable per capita consumption of fresh water, leading to overexploitation of groundwater and consequent drawdown of its level [4]. The resulting alteration of the freshwater/seawater interface facilitates saline wedge advancement and the up-coning of saltwater under the extraction wells [1,5,6], which lead to seawater intrusion (SWI) and eventually the salinization of coastal aquifers. SWI affects almost all coastal aquifers around the world to different degrees [2,5,7] and also those in the Mediterranean region [8–10], causing deterioration of groundwater quality with detrimental effects on surface water and related ecosystems, in addition to hindering the use of groundwater for human purposes. This state can persist even a long time after the groundwater pumping has been stopped because an aquifer may require a long period to recover its initial state [11]. In addition to the overexploitation, SWI can be

due to the reduction of recharge and resulting freshwater decrease [12,13] consequent to both natural phenomena, such as changes in precipitation and evapotranspiration regimes related to climate change and anthropic pressures, like growing urbanization, river regulation, marsh reclamation, and the rising use of water-saving irrigation systems which reduce the infiltration rates [14,15]. Generally speaking, apart from the SWI, the salinity of groundwater results from the overlaying of complex processes involving different sources, such as the composition and amount of precipitation, the irrigation water, and the disposed wastewater, as well as water–rock interaction, the paleo-seawater, the marine aerosol and geothermal sources, among others [1,3,16–20]. To date, various studies have been conducted to understand the sources of salinization in coastal areas [3,21,22].

Hydrogeochemical characterization of groundwater through major ions and trace elements supplemented by the analysis of characteristic ion ratios is a frequently used approach [16–19,23–27]. Indeed, the comparison of some characteristic ion ratios (such as Na/Cl, Cl/HCO<sub>3</sub>) observed in groundwater with that observed in seawater, represents a useful method to discriminate groundwater affected by seawater mixing from that not affected by this phenomenon. Other characteristic ion ratios (such as Ca/HCO<sub>3</sub>) allow putting a boundary between the groundwater influenced by water–rock interaction (e.g., by the dissolution of calcite and dolomite) and that influenced by mixing with seawater. However, these characteristic ion ratios fail to identify the contribution of paleo-seawater which can however be tackled with the support of environmental isotopes [28–31], that enable identification of the different contributions of modern seawater, paleo-seawater, and water–rock interaction to the groundwater salinity because of the typical isotopic fingerprint that characterizes these different sources of ions. Statistical and geostatistical analyses have been introduced to group groundwater influenced by the same processes [18,24,27,32]. Finally, geochemical modelling integrated with hydrogeochemical characterization [1,33,34] and statistical analysis [35] allows modelling of water–rock interaction processes and the mixing with seawater. The above-described methodologies have been combined at different degrees of integration to explain the salinization process in coastal aquifers.

In this paper, an integrated approach is presented in which all the steps described above as well as the mixing calculation are applied to investigate the processes that govern the spatial salinity variation of groundwater in the karstic aquifer of Coastal Murgia (Apulia, southern Italy), from the upland recharge areas to the lowland zone. This work aims to demonstrate that this integrated approach is a robust method that allows identification of the different salinity sources and their contribution to the salinity of the study area, and assessment of the contribution of mixing between the different end-members, and water–rock interaction processes in the hydrogeochemical evolution of groundwater. Overcoming the limitations of the individual approaches, the integrated application of all investigation methods can lead to a clear definition of a conceptual model and an appropriate identification of salinization sources.

## 2. Materials and Methods

### 2.1. Study Area

Coastal Murgia (1227 km<sup>2</sup>) is a coastal groundwater body located in Apulia (southern Italy). It is part of a wider fractured and karstified calcareous-dolomitic aquifer (Murgia aquifer) hosted in the Upper Jurassic–Cretaceous carbonate formations of the Apulian Platform (Figure 1). The Murgia area is characterized by the presence of thick, well-bedded, carbonate facies, overlain by discontinuous and thin Late Pliocene–Quaternary deposits belonging to the Bradanic Trough sedimentary cycle [36]. Clay-rich deposits (bauxite and terra rossa), representing the residual material of carbonate rocks weathering, can be found both as lenses interbedded in the carbonate sequence or as materials filling karst cavities [37,38].

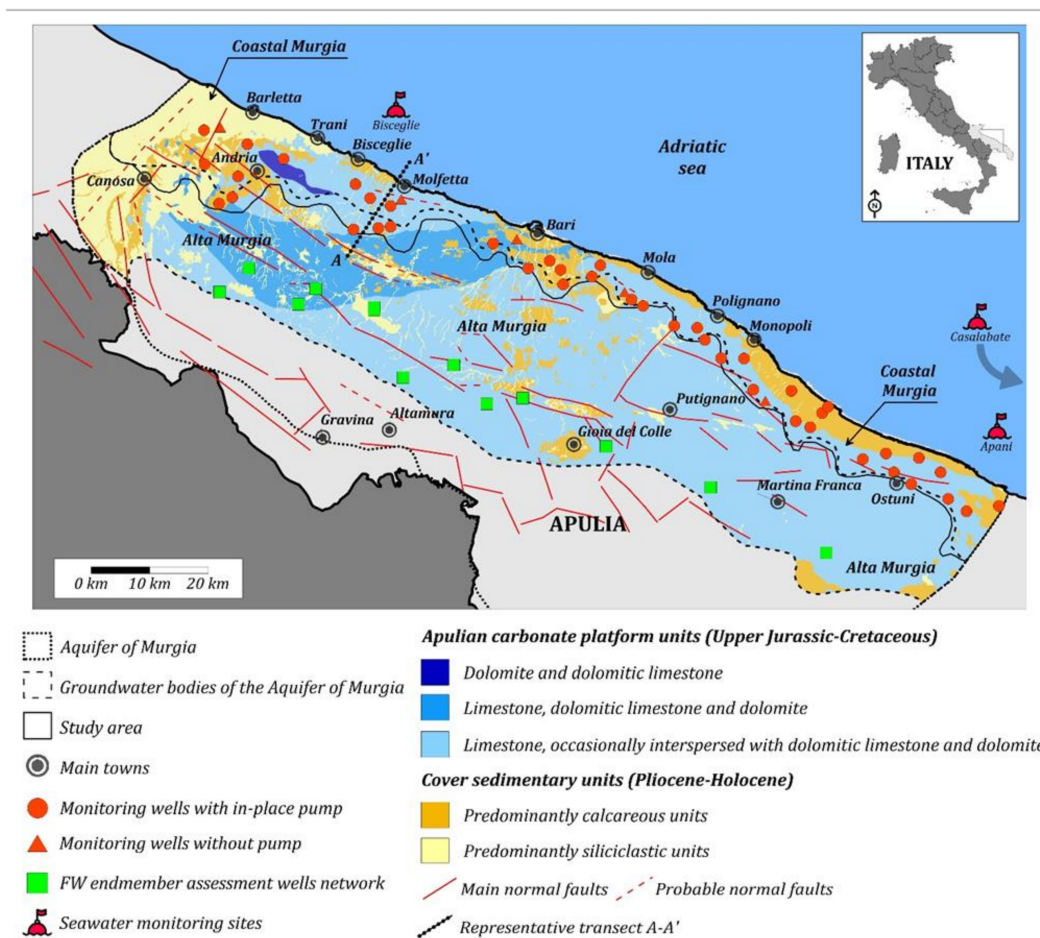


**Figure 1.** Geological map of Coastal Murgia and current monitoring network.

The aquifer has an irregular geometry due to the presence at different depths of thick dolomitic layers that, having lower permeability, force groundwater to flow under variable confinement conditions. However, the aquifer is phreatic in the coastal strip, although also in this area confined conditions can be locally observed [39,40]. Moreover, the discontinuous karstification and inhomogeneous fracturing affecting the rocks make the aquifer markedly anisotropic with a very variable permeability both in the horizontal and vertical dimensions [41]. In the Murgia aquifer, freshwater floats on the saltwater that penetrates the mainland and flows to the Adriatic Sea through both diffuse-discharge and discrete type springs [39].

According to the Köppen–Geiger Climate Classification System [42], the study area belongs to the Csa climate zone, known as the Mediterranean Climate, corresponding to a warm temperate climate with dry and hot summers and mild, wet winters. The yearly precipitation average is about 600 mm, mainly concentrated in the months of November–February [43,44]. Local precipitation recharges the Coastal Murgia by infiltration and the latter is also fed by the Alta Murgia (3842 km<sup>2</sup>) aquifer located upstream.

## 2.2. Groundwater Sampling and Field Analyses

The groundwater of Coastal Murgia was sampled in autumn 2019 using a specifically defined monitoring network. This monitoring network consists of 47 existing wells, 42 of which are equipped with in-place pumps. The depth of monitoring wells (MWs) and the depth of screen have a wide variation range (Table S1) and their distance from the coastline is between 0.7 and 16.7 km (Figure S1). The MWs are generally sealed and the piezometric head cannot be measured.

According to standardized sampling protocols [45], the 42 monitoring wells (MWs) equipped with a pump were purged until chemical–physical parameter stabilization (dissolved oxygen, oxidation–reduction potential, temperature, pH, and electrical conductivity), which was verified by AQUAREAD probe measuring. In the five remaining MWs (Table S1) sampling was performed using a Nansen bottle-type 1.2 L water sampler without purging, at a depth corresponding to the bottom of the freshwater lens, identified by a vertical log of the electrical conductivity performed with an Idronaut Ocean Seven 303 multiparameter probe.

The concentrations of ammonium, nitrites, and cyanides were measured on-site by UV–Vis spectrophotometry (Spectrophotometer DR1900 Hach-Lange).

Samples for inorganic compounds (anions, cations, and trace elements) were filtered (0.45 µm pore size polycarbonate filters) on-site and stored in HDPE bottles previously washed with HNO<sub>3</sub> and rinsed with Milli-Q water. Samples for cation and trace element analyses were in addition acidified on-site with HNO<sub>3</sub> at pH < 2. Samples for dissolved organic carbon (DOC) analysis were filtered (0.7 µm pore size glass microfiber filters) and acidified (HCl) on-site and stored in pre-treated HDPE bottles.

Raw samples for isotope analysis (<sup>87</sup>Sr/<sup>86</sup>Sr) were collected in HDPE bottles.

### 2.3. Lab Analyses

Major anions analysis with ion-exchange chromatography (Thermo Scientific™ Dionex™ Aquion™ IC) (Table S2) and HCl titration (Hach-Lange TitraLab AT1000) for alkalinity determination were performed within 24–72 h.

Cations and trace elements were analysed within 1 month with ICP-mass spectrometry (Agilent technologies 7500 c) (Table S2). The analytical performance of ICP-MS was tested against a certified material (NIST 1640a, trace elements in natural waters).

Dissolved organic carbon was determined with the Shimadzu TOC-5000A analyser.

Isotope analysis of strontium required sample purification using Bio-Rad micro-columns with Eichrom Sr-spec resin (100–150 µ). Isotope analyses were performed using Thermo Fisher Scientific Neptune plus™ MC-ICP-MS equipped with a Scott-type spray chamber in quartz, with 100 µL/min flux cyclonic nebulizer, 10<sup>−11</sup> Ohm resistors for <sup>88</sup>Sr, <sup>87</sup>Sr, and <sup>86</sup>Sr measurement, and 10<sup>−12</sup> Ohm for <sup>85</sup>Rb, <sup>84</sup>Sr, and <sup>83</sup>Kr. Samples were run at <sup>88</sup>Sr signal ranging from 7 to 12 Volts, with a negligible signal of the blank (<5 mV). The average <sup>87</sup>Sr/<sup>86</sup>Sr ratio of the NIST SRM 987 standard measured during samples analysis was 0.710249 ± 0.000020 (n = 10).

The electro-neutrality (EN%), calculated using Equation (1) was contained within 5% [46]

$$EN\% = 100 * \frac{(\sum cations - \sum anions)}{(\sum cations + \sum anions)} \quad (1)$$

### 2.4. Multivariate Statistical Methods

Principal component analysis (PCA) based on the correlation matrix of the variables (major ions and some significant minor elements, such as lithium, boron, strontium, and rubidium) was run to summarise the hydrochemical features of the dataset and investigate possible main processes. In addition, hierarchical clustering using the UPGMA aggregation algorithm (unweighted pair group method with arithmetic mean) was performed to identify groundwater with homogeneous characteristics, dividing them into statistically significant groups. As for the PCA, the cluster analysis was carried out using the correlation matrix of the major ions as a similarity measure. The multivariate analysis was performed with the software PAST (version 3.20; [47]).

### 2.5. Mixing Calculations

The seawater fraction ( $f_{\text{sea}}\%$ ) in Coastal Murgia groundwater samples was estimated according to the mass balance in a two end-members system, using the chloride concentration in Equation (2) [48,49]:

$$f_{\text{sea}}(\%) = \frac{m_{\text{Cl}} - m_{\text{Cl,FW}}}{m_{\text{Cl,SW}} - m_{\text{Cl,FW}}} * 100 \quad (2)$$

where  $m_{\text{Cl,FW}}$  and  $m_{\text{Cl,SW}}$  represent chloride concentration in the freshwater and seawater end-members respectively, while  $m_{\text{Cl}}$  is the concentration in a groundwater sample.

As freshwater chloride end-member, the median of the chloride concentration values measured in the Alta Murgia groundwater body (the inland recharge areas) has been calculated. In particular, these values were derived from sampling conducted in 13 monitoring wells (green squares in Figure 1) during the previous monitoring (2007–2018) carried out by the Apulia Region [50]. The seawater chloride end-member is the median of the chloride concentration values of the Adriatic Sea collected in three seawater monitoring sites within another research activity (M.D. Fidelibus, personal communication, January 2020) (Figure 1).

### 2.6. Geochemical Modelling

Aqueous geochemical calculations were performed with PHREEQC Version 3 [51] to model the processes responsible for the observed groundwater chemistry. In particular, the software was used to simulate in a batch experiment the theoretical mixing of the two end-members, calculated as above, for the main parameters ( $\text{Cl}^-$ ,  $\text{SO}_4^{2-}$ ,  $\text{Br}^-$ ,  $\text{Na}^+$ ,  $\text{Ca}^{2+}$ ,  $\text{Mg}^{2+}$ ,  $\text{K}^+$ ,  $\text{HCO}_3^-$ ).

The mixing of the two end-members was also simulated in the presence of an unspecific exchanger (e.g., clay mineral). Assuming a mainly calcic composition of an exchanger in a karst aquifer, the exchanger was placed in equilibrium with the FW end-member (Ca- $\text{HCO}_3$  groundwater), to define its initial assemblage. The mixing process was then simulated to evaluate the deviation from the pure mixing lines caused by the cation exchange processes.

Finally, a specific simulation was performed at a representative transect (A-A'), defined across MWs 13, 27, and 29 in the northwestern area (Figure 1), to simulate the main processes responsible for the geochemical evolution of groundwater from the recharge areas towards the coast. In this simulation, more specific end-members were calculated using the median of the concentration values of the five northernmost of the above-mentioned Alta Murgia monitoring wells in the recharge area, and the northernmost point (Bisceglie) in the Adriatic Sea. The simulated geochemical processes along the transect A-A' include the equilibrium reactions of carbonate minerals, cation exchange, and mixing with seawater at various percentages. In detail, starting from the composition of the FW end-member, the geochemical modelling was applied to the following:

- dissolution reactions via sequential adaptation of the saturation indexes of selected mineralogical phases (calcite, dolomite, strontianite) to those of the groundwater sampled along the transect (MWs 13, 27, and 29);
- calculation of the exchange assemblage in equilibrium with the FW end-member and progressive readjustment to subsequent solutions;
- FW-SW mixing at the percentages identified for the three selected samples.

## 3. Results and Discussion

The Piper diagram (Figure 2) shows an evolution from bicarbonate types toward waters progressively closer to the seawater composition, the only exception being sample 32 which falls into the field of the alkaline bicarbonate waters. This sample also shows anomalies for other parameters, such as high  $\text{NH}_4^+$  (1.13 mg/L) and DOC (11 mg/L), suggesting possible anthropogenic contamination; therefore, it was removed from the

dataset in the statistical elaborations. In the other MWs, the  $\text{NH}_4^+$  concentration was generally below the detection limit (0.02 mg/L) or ranged between 0.021 and 0.244 mg/L, while DOC was between 0.4 and 1.7 mg/L.

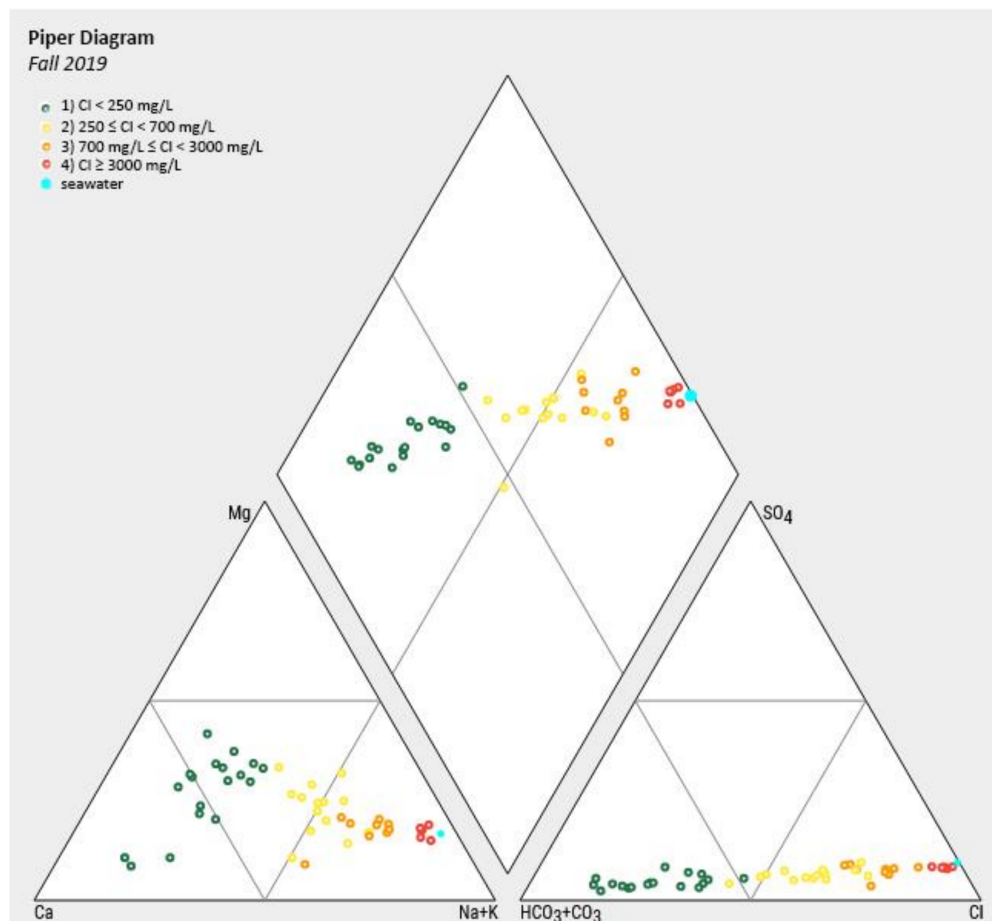


**Figure 2.** Piper diagram showing major groundwater components of Coastal Murgia in autumn 2019.

The chloride concentration varies in a very wide range (39–9684 mg/L) (Table S3). Based on the chloride concentration, samples were divided into four groundwater groups (Table S4): (1)  $\text{Cl}^- < 250$  mg/L, (2)  $250 \leq \text{Cl}^- < 700$  mg/L, (3)  $700 \text{ mg/L} \leq \text{Cl}^- < 3000$  mg/L, (4)  $\text{Cl}^- \geq 3000$  mg/L. The variability of chloride is reflected in the electrical conductivity (EC) which ranges between 711 and 19590  $\mu\text{S}/\text{cm}$  (Table S3).

The PCA results show that the first two principal components explain 89.6% of the total variance (80.3% and 9.3% by the first and second components respectively) (Figure 3a). The positive loadings of PC1 highlight the important contribution of almost all major ions, except  $\text{HCO}_3^-$  which is relatively low in seawater. Together with major ions, there are also minor elements characterized by high residence times and normally more abundant in seawater (lithium, boron, strontium, rubidium), suggesting that PC1 is related to FW-SW mixing. The second component is mainly linked to two different factors. Negative values of PC2 are linked to the contribution of  $\text{HCO}_3^-$  and allow for individual MWs influenced by water-rock interaction processes, in particular the interaction with carbonate rocks (dolomitized limestones and dolomites). Positive loadings of PC2 highlight the contribution of  $\text{NO}_3^-$  and allow identification of MWs characterized by groundwater affected by anthropic activities, in particular the intensive land use for agricultural purposes.

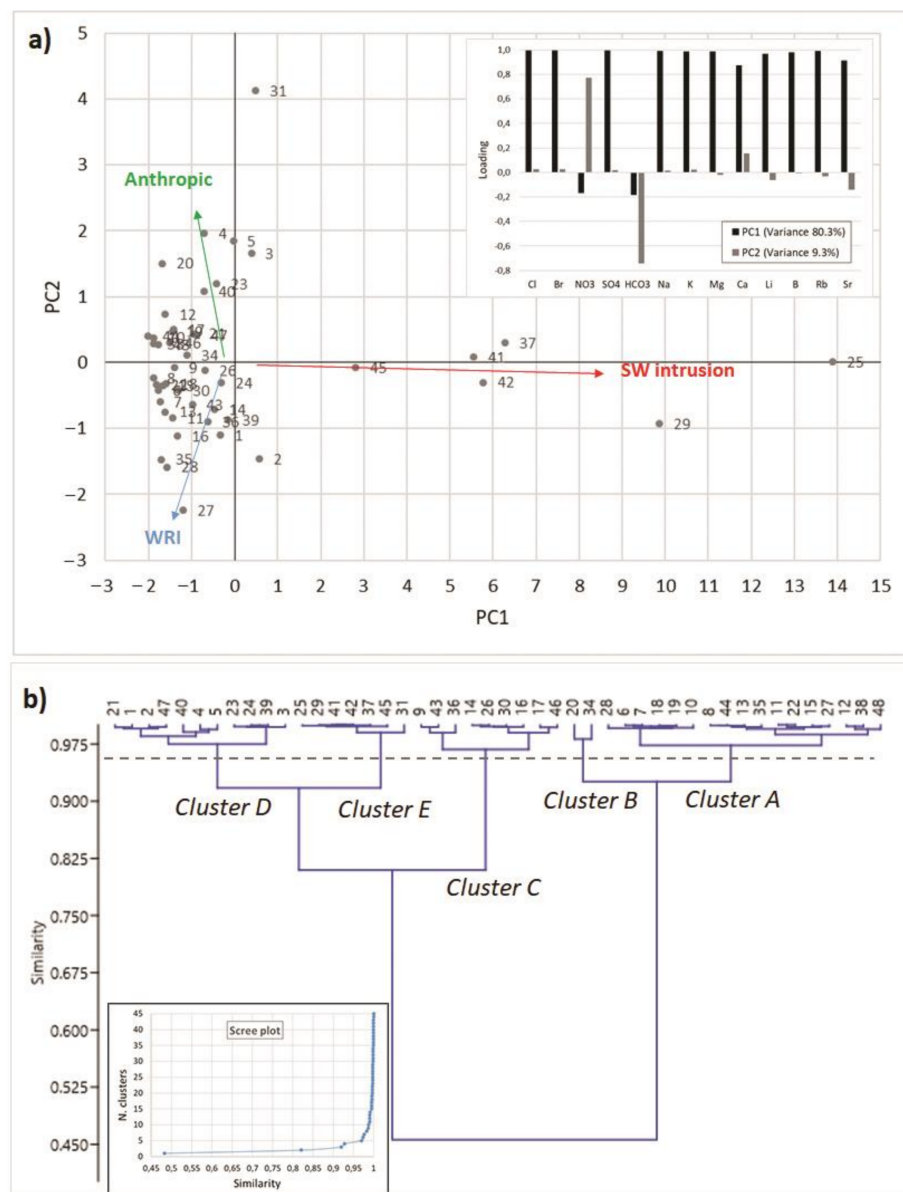


**Figure 3.** (a) Principal component analysis, (b) cluster analysis. WRI = water-rock interaction, SW Intrusion = seawater intrusion.

Hierarchical clustering performed on the major ions enable five clusters (Figure 3b) to be recognized. The choice of the number of significant clusters was based on the linkage distance analysis (similarity measure). In particular, the scree plot suggests maintaining a subdivision into five clusters, since for further subdivisions an evident relative decrease of similarity is observed. The five clusters identified more or less overlap the subdivision in the groups based on chloride concentration (Table S4), from cluster A (low salinity) to cluster E (high salinity), the latter containing the same MWs identified also in the PCA scatterplot (PC1, Figure 3a). Cluster B consists of only two samples (20 and 34) showing concentration of chlorides at the boundary between groundwater groups 1 and 2 (233 and 289 mg/L, Table S4). These two samples hence define a separate small cluster in the dendrogram (Figure 3b).

The highest chloride concentration was observed near the coastline (within 3 km) and a general decrease is observed from the coast to the inland. However, different chloride concentrations (up to more than two orders of magnitude) can be observed in MWs located at the same distance from the coastline and in adjacent areas (Figure S1). This latter

phenomenon suggests that other factors may influence the salinity of the samples, such as the high hydraulic properties anisotropy, the different MWs depths, and the presence of seawater intruded into aquifers during the different sea level rises occurring in the South-Apennines Foreland, during the Pleistocene glacial periods [52,53].

To understand the main sources of salinity, mixing calculation, characteristic ion ratios ( $\text{Na}/\text{Cl}$ ,  $\text{Cl}/\text{HCO}_3$ ,  $\text{Ca}/\text{HCO}_3$ ), simulations of mixing and water-rock interaction, and isotope analysis were performed.

As expected, the mixing calculation shows an increase in the seawater fraction ( $f_{\text{sea}}\%$ ) in the groundwater samples with the highest EC values and chloride concentrations (Table S4). The samples belonging to groundwater groups 1 and 2 show that the  $f_{\text{sea}}\%$  is generally low (maximum 3.3%) with tight ranges (maximum about 2% in group 2). Groundwater samples of groups 3 and 4 have  $f_{\text{sea}}\%$  in the ranges 3.7–8.6% and 16.4–50.6% respectively, showing a greater variability than the other groups.

Figure 4a shows the comparison of the theoretical mixing line between the two end-members with the observed values for those parameters ( $\text{Cl}^-$ ,  $\text{SO}_4^{2-}$ ,  $\text{Br}^-$ ,  $\text{Na}^+$ ,  $\text{Mg}^{2+}$ ,  $\text{K}^+$ ) more impacted by seawater intrusion ( $\text{SW}/\text{FW} \geq 30$ ). The samples with  $f_{\text{sea}}\% > 5\%$  follow the trend of the simulated mixing curves, in particular for  $\text{Mg}^{2+}$ ,  $\text{Na}^+$ ,  $\text{Br}^-$  and  $\text{SO}_4^{2-}$ , although slightly lower. The good fit is gradually lost when the mixing percentage becomes lower, except for  $\text{Na}^+$  and  $\text{Br}^-$  for which a good agreement remains. Other removal or enrichment processes can cause fluctuations with respect to the pure mixing with seawater. For example, at low mixing percentages,  $\text{Mg}^{2+}$  shows higher concentrations than the theoretical mixing curve, probably related to water–rock interaction (dissolution of dolomites and dolomitic limestones). Regarding  $\text{Ca}^{2+}$  ( $\text{SW}/\text{FW} = 4$ ) and  $\text{HCO}_3^-$  ( $\text{SW}/\text{FW} = 0.3$ ), less enriched in seawater, the mixing processes have less influence, and only at a particularly high mixing percentage, is there a certain agreement with the theoretical curves, although an excess of  $\text{Ca}^{2+}$  concentrations is observed (Figure 4b). This excess can derive from the water–rock interaction with clay minerals and consequent ion exchange processes during mixing phenomena. It is known that calcium excess with respect to bicarbonate can be attributed to the reverse ion exchange process during seawater intrusion [24]. As regards bicarbonates, a dilution is observed moving towards higher mixing percentages due to the modest bicarbonate concentration in the seawater.

Characteristic ion ratios can be useful to understand the origin of salinization and in this paper,  $\text{Na}/\text{Cl}$  and  $\text{Cl}/\text{HCO}_3$  ratios were considered (Table S4). The  $\text{Na}/\text{Cl}$  ratio can be used as an indication of SWI or to unveil sorption/desorption processes during seawater intrusion/refreshing [48].

Generally, values of  $\text{Na}/\text{Cl}$  ratio lower than those of SW end-member (0.90) were observed for MWs with  $f_{\text{sea}} \geq 0.5\%$  (Table S4). These values are indicative of seawater intrusion; indeed, during the seawater intrusion sodium exchange occurs while chloride, since it is conservative, is not affected by the ion exchange processes, and the  $\text{Na}/\text{Cl}$  ratio decreases, becoming lower than the typical ratio of seawater [48,54]. In the MWs with  $f_{\text{sea}} < 0.5\%$ , instead, values higher than the typical SW end-member ratio were in general observed, indicating a lack of seawater intrusion or else refreshing because the absorbed sodium is released while calcium becomes absorbed [48] (Table S4). In some MWs, especially those characterized by low mixing percentage,  $\text{Na}/\text{Cl}$  ratios higher than 1 were observed, indicating, according to Jiao and Post [48], possible contamination by anthropogenic sources; however, the other possible indicators of anthropic impacts, such as  $\text{NH}_4^+$  and DOC, do not diverge from other samples. The  $\text{Cl}/\text{HCO}_3$  ratio remarks what is indicated by  $\text{Na}/\text{Cl}$  ratio (Table S4); indeed, also the  $\text{Cl}/\text{HCO}_3$  ratio indicates no or negligible seawater intrusion in the MWs with  $f_{\text{sea}} < 0.5\%$  and characterized by  $\text{Na}/\text{Cl} > 0.90$ . Instead, the MWs with  $\text{Na}/\text{Cl}$  ratio  $< 0.90$  show the  $\text{Cl}/\text{HCO}_3$  ratio in the range typical of groundwater affected by seawater intrusion. Particularly, based on  $\text{Cl}/\text{HCO}_3$  range limits found in the literature [55,56] it is possible to distinguish water affected by increasing degrees of seawater intrusion: slightly ( $0.5 < \text{Cl}/\text{HCO}_3 < 1.3$ ), moderately ( $1.3 < \text{Cl}/\text{HCO}_3 < 2.8$ ), injuriously ( $2.8 < \text{Cl}/\text{HCO}_3 < 6.6$ ) and highly affected ( $\text{Cl}/\text{HCO}_3 > 6.6$ ) (Table S4).

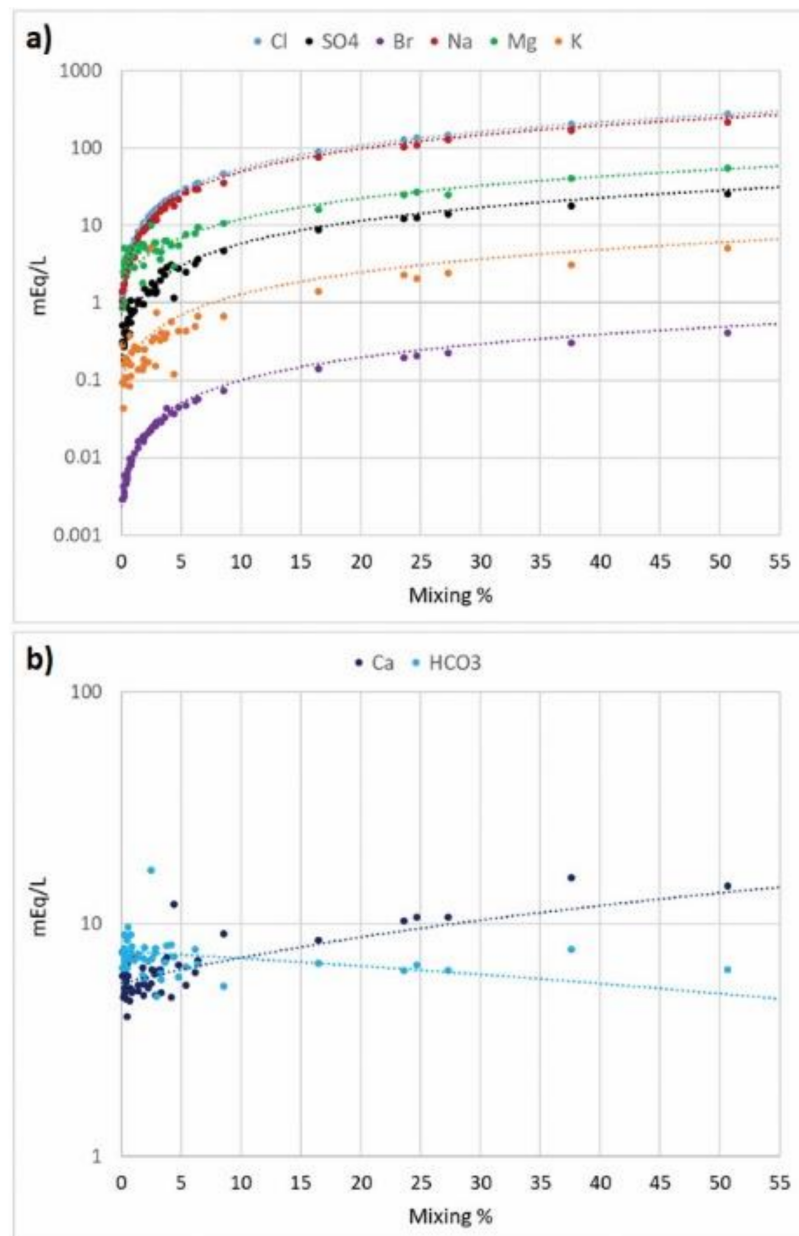


**Figure 4.** (a) Concentration trends of the parameters more influenced by seawater intrusion (SW/FW  $\geq$  30), (b) parameters less influenced by seawater intrusion (SW/FW  $\leq$  4). Dotted lines represent the simulated mixing of the two end-members, while points represent the concentrations observed at the sampling points (mixing percentage calculated by Equation (2)).

The isotope ratio  $^{87}\text{Sr}/^{86}\text{Sr}$  was used to study the origin of groundwater salinity because it allows recognition of the fingerprint of hosting rocks, modern seawater, and paleo-seawater. For this study, a representative sub-set consisting of 15 MWs was chosen from a wider dataset [57]. A few MWs are characterized by high  $f_{\text{sea}}\%$  and strontium concentration and an  $^{87}\text{Sr}/^{86}\text{Sr}$  ratio tending to, even though not reaching, the current seawater value (0.70918) [58]. These MWs can be considered affected by current seawater intrusion (Figure 5a and Figure S2). The study allowed exclusion of the presence of paleo-seawater from the Cretaceous period, which is characterized by an isotope ratio ranging from 0.7073–0.7078 [59] and a strontium concentration from 8.0–40.0 mg/L (Figure S2) [60,61]. Nevertheless, further studies are ongoing to evaluate the presence of paleo-seawater from other epochs. Finally, the four MWs belonging to group 1 in Table S4, are all characterized by lower  $f_{\text{sea}}\%$  and Sr concentration and similar ion ratios. In

particular, the  $\text{Cl}/\text{HCO}_3$  and  $\text{Na}/\text{Cl}$  ratio values in such MWs indicate a very low influence of seawater intrusion, while the  $\text{Ca}/\text{HCO}_3$  values suggest groundwater is influenced by water-rock interaction (Table S4, Figure S3). Nevertheless, the MW7 behaves differently from the other three with regard to the  $^{87}\text{Sr}/^{86}\text{Sr}$  ratio. Actually, the other three MWs are characterized by an isotopic ratio within the range typical of the Apulian Cretaceous platform (0.7073–0.7078), whilst the related MW7 value is slightly above the upper limit of this range (Figure 5 and Figure S2) [59]. This different behaviour of MW7 can be explained by supposing shorter residence times of groundwater intercepted by this well, which would indicate a less significant water-rock interaction. Differently from the other three wells which are clustered on the northwest side of the study area, characterized by rather compact limestones and dolostones, the MW7 is located on a fractured and karstified area, about 60.0 km south-east. Tulipano et al. [41] confirm such an assumption indicating slow flow circuits on the northwest side and faster circuits on the opposite southeast side of the study area (Figure 5b).

Based on the above analyses, which indicate a significant contribution of bicarbonates in the MWs located in the northwestern sector of the study area (negative PC2), the transect A-A' in Figure 5 has been outlined to simulate the geochemical groundwater evolution while it flows from the recharge area to the sea. The transect starts with the assumed FW end-member value, in the inner end, and finishes with the related SW value at the sea after passing through the MW numbers 13, 27, and 29, located at a decreasing distance from the coast.

Before carrying out the geochemical modelling of the groundwater quality evolution along the transect A-A', similar modelling was performed including all the MWs, to simulate the contribution of water-rock interaction with respect to mixing with seawater. In Figure 6a it is possible to observe how the samples showing significant mixing with seawater (>3%) are all below the pure mixing line obtained by geochemical modelling, both for  $\text{Na}^+$  and  $\text{K}^+$ . Simulating the presence of an unspecific exchanger (from 25 to 100 mmol/kg water), the mixing lines seem to better approximate the trend of groundwater samples. The use of a generic exchanger is due to the lack of knowledge of the specific exchange phase involved in the process (clay mineral) and, consequently, of its cation exchange capacity. The results confirm that mixing phenomena in the aquifer are probably accompanied by ion exchange processes that remove alkali from the groundwater. On the other hand, calcium tends to show higher values than theoretical mixing (Figure 6b). The coupling of mixing and ion exchange processes, however, determines a significant increase of concentration in solution and none of the possible scenarios seems to fit with the field data (Figure 6b). The calculated solutions are particularly supersaturated in calcite compared to pure mixing and the groundwater samples themselves (Figure S4). This suggests how mixing and ion exchange processes can induce metastable imbalance conditions, with an excess of calcium and consequent precipitation of  $\text{CaCO}_3$ , predictably until the chemical equilibrium is restored. This hypothesis agrees with the simulations of Appelo and Willemsen [62] and Appelo [63], who adopted the equilibrium with calcite as a constraint on the increase of calcium concentrations in simulating the seawater intrusion in a freshwater aquifer.

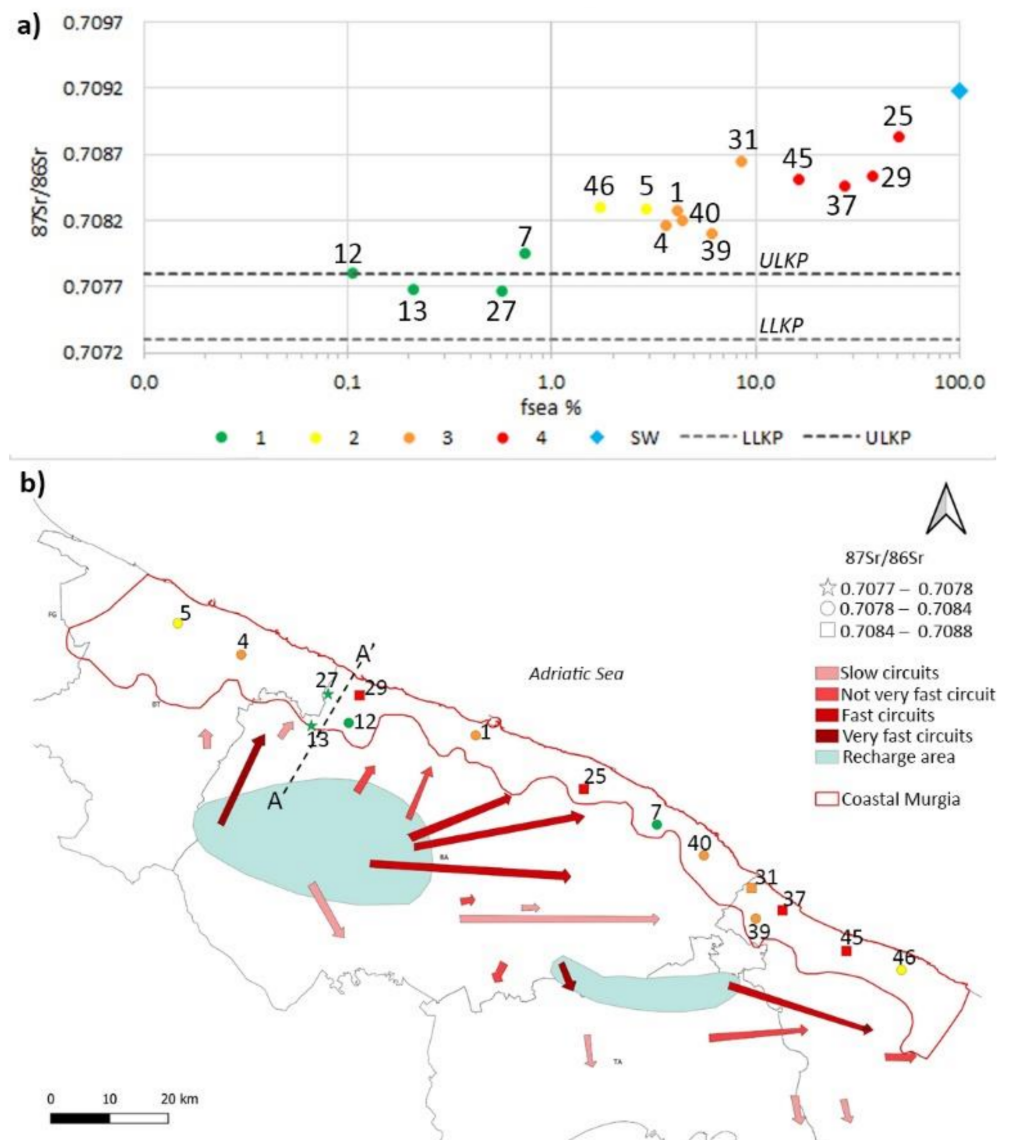
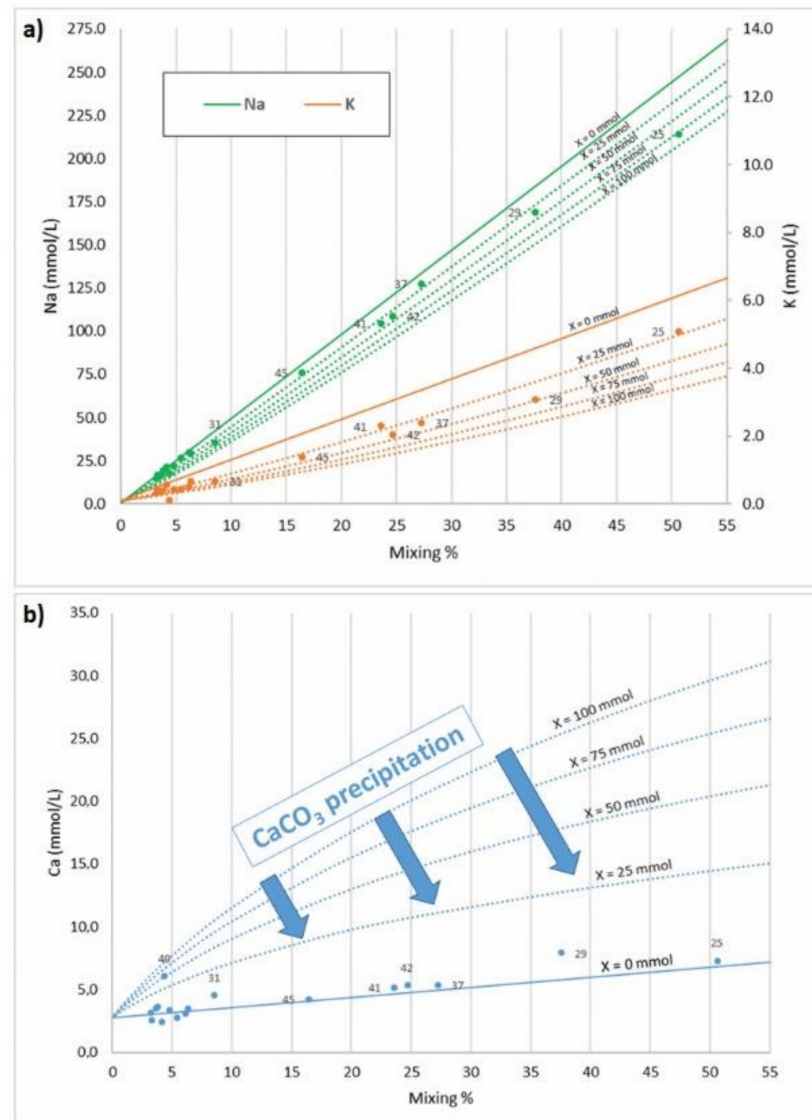


**Figure 5.** (a)  $^{87}Sr/^{86}Sr$  ratio vs  $f_{sea}$  % observed in the MWs of the Coastal Murgia. Different dots represent different groundwater groups: green (1) groundwater with  $Cl^- < 250$  mg/L, yellow (2) groundwater with  $250 \leq Cl^- < 700$  mg/L, orange (3) groundwater with  $700 \text{ mg/L} \leq Cl^- < 3000$  mg/L, red (4) groundwater with  $Cl^- \geq 3000$  mg/L. The light blue diamond represents the value of the current seawater. ULKP = upper limit of the Cretaceous platform, LLKP = lower limit of the Cretaceous platform.; (b) map of  $^{87}Sr/^{86}Sr$  ratio observed in the MWs. Symbol colours are the same as above defined. Different shapes (stars, dots, and squares) represent different ranges of  $^{87}Sr/^{86}Sr$  values. Arrows and recharge areas modified from Tulipano et al. [41]. The dashed black line represents the representative transect A-A' chosen for simulation.

As introduced above, the transect A-A' (Figure 5b) was chosen to simulate the main processes responsible for the geochemical evolution of groundwater, starting with the two end-members FW and SW.

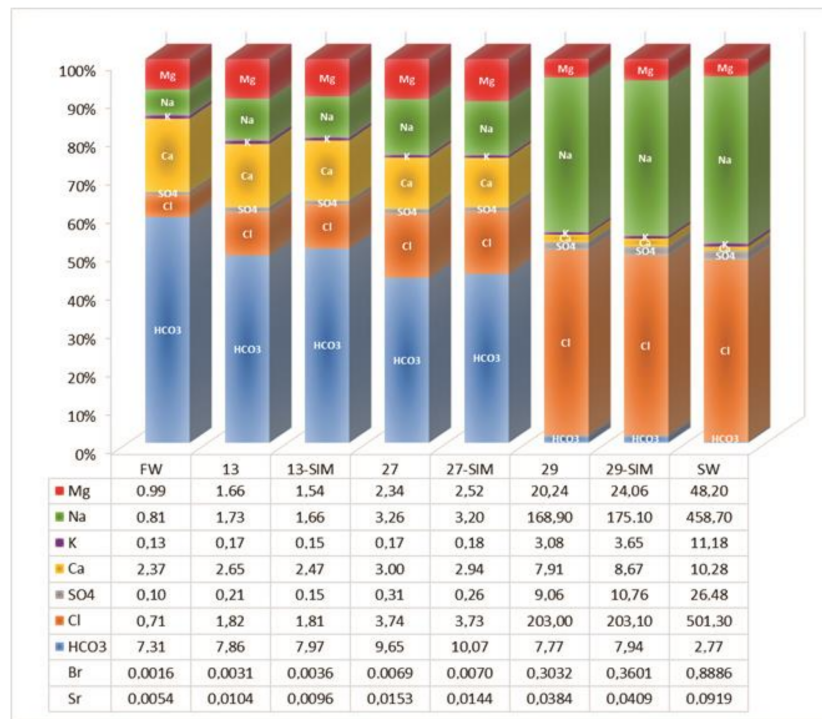
The simulated geochemical processes include the equilibrium reactions of carbonate minerals (calcite, dolomite, strontianite), ion exchange ( $25 \text{ mmol } X^- / \text{kg water}$ ), and mixing with seawater. Groundwater in the study area is at the saturation limit with respect to calcite and dolomite, while it shows an evident undersaturation in strontianite (Figure S5). The software uses a database file of thermodynamic data derived from WATEQ4F [64] which contains pure mineralogical phases. Rather than as a pure phase, Sr is generally present as trace element in carbonate minerals. Its presence in these minerals may be

an important source of this element in groundwater, but its effect on the equilibrium of calcite is generally small [65]. Consequently, instead of pure strontianite, the existence of a  $\text{CaSrCO}_3$  phase, equally close to equilibrium, is more likely.



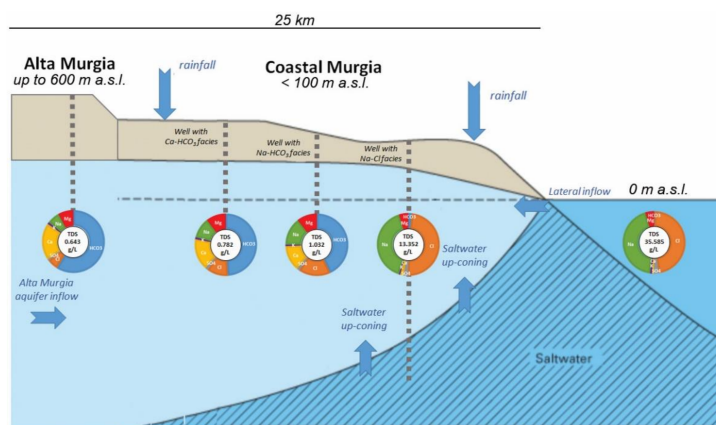
**Figure 6.** Comparison between pure mixing (continuous line) and simulated concentrations obtained coupling the model mixing + ion exchange (dotted lines) at different exchanger concentrations. (a) Na and K (left and right ordinate scale, respectively); (b) Ca.

Figure 7 shows the result of the simulation along the transect A-A'. Simulated concentrations are quite similar to the analytical values of the three MWs for all major ions, bromide and strontium, with a mean error of 8.5%, ranging from a minimum of 2.7% for  $\text{HCO}_3^-$  and a maximum of 20.6% for  $\text{SO}_4^{2-}$ . These results confirm the goodness of the hypothesized geochemical processes. In the aquifer, further processes could act on these and other minor elements (e.g., dissolution/precipitation of other mineralogical phases, sorption/desorption processes on Fe oxy-hydroxides, rainfall/aerosol contribution in the coastal area), causing possible variations with respect to the simulated concentrations.



**Figure 7.** Variation of the groundwater chemistry along the selected transect A-A'. The % of major ions measured in the three wells (13, 27, and 29) and the simulated values (13-SIM, 27-SIM, and 29-SIM) are represented. The table below shows the concentrations in mmol/L, also for bromide and strontium. FW = freshwater end-member; SW = seawater end-member.

The selected transect is particularly suitable for this type of simulation and the identified processes can be extended to the entire groundwater body. The integrated approach allowed us to improve the conceptual model of the Coastal Murgia groundwater body and identify the possible sources of salinization (Figure 8). The Coastal Murgia groundwater body is mainly recharged by the Alta Murgia groundwater body characterized by Ca-HCO<sub>3</sub> water. In the Coastal Murgia this groundwater evolves towards waters progressively closer to the seawater composition. Indeed, as shown in Figure 8, moving from inland to the coastline the groundwater becomes Na-HCO<sub>3</sub> and Na-Cl due to the mixing phenomena and consequent ion exchange processes accompanied by calcite precipitation.



**Figure 8.** Schematic conceptual model (not in scale) of the investigated area. In the doughnut charts: blue = HCO<sub>3</sub><sup>-</sup>, orange = Cl<sup>-</sup>, grey = SO<sub>4</sub><sup>2-</sup>, yellow = Ca<sup>2+</sup>, purple = K<sup>+</sup>, green = Na<sup>+</sup>, red = Mg<sup>2+</sup>.

#### 4. Conclusions

The combination of diverse methods of groundwater quality data interpretation can be effective for quantifying the degree of salinization and discriminating its different sources.

Chemical facies characterization, multivariate statistical analysis, and mixing calculation proved to be effective to quantify the groundwater salinization degree up to 50% in the study area. A further in-depth analysis exploiting the characteristic ion ratios and pure mixing calculation permitted current seawater intrusion as a main source of salinization to be individuated. Cretaceous paleo-seawater as an additional source of salinization was excluded based on the  $^{87}\text{Sr}/^{86}\text{Sr}$  results obtained on a subset of monitoring wells. In addition, the  $^{87}\text{Sr}/^{86}\text{Sr}$  and the  $\text{Ca}/\text{HCO}_3$  ratios enabled us to identify water-rock interaction as a driver of the geochemical evolution of groundwater and this hypothesis was verified by geochemical modelling.

The study evidenced two main processes responsible for the groundwater chemistry evolution from inland to the coast in the study area: Water–rock interaction within the carbonate aquifer (dissolution and ion exchange processes with clay minerals) and mixing with seawater caused by the current saline intrusion.

Further isotope data for  $^{11}\text{B}$ ,  $^{18}\text{O}$ ,  $^2\text{H}$ ,  $^{87}\text{Sr}/^{86}\text{Sr}$  to support water/rock interaction and mixing processes are in preparation.

The proposed approach can be successfully applied to coastal karst aquifers for the investigation of the main processes governing the salinity variation in groundwater, to support more informed management of the groundwater and the improvement of its quality. However, the applied methodologies can also be adopted in a different geological context, making the appropriate changes (e.g., choice of suitable isotopes, different mineralogical phases, and the reactions to be included in the geochemical model) to adapt them to the specific case studies.

**Supplementary Materials:** The following supporting information can be downloaded at: <https://www.mdpi.com/article/10.3390/w14111725/s1>, Figure S1. Map of chloride concentrations and chart of chloride concentrations vs distance from coastline; Figure S2.  $^{87}\text{Sr}/^{86}\text{Sr}$  ratio vs Sr concentration observed in the MWs of the Coastal Murgia. The meaning of dots colours is the same of the figure S1. The light blue diamond represents the value of the actual seawater. ULKP = upper limit of the Cretaceous platform, LLKP = lower limit of the Cretaceous platform. Blue rectangle represents the range of paleo-seawater; Figure S3. Map of chloride concentration at the monitoring wells and the spatial interpolation of  $\text{Ca}/\text{HCO}_3$  ratio (Inverse Distance Squared Weighted method). Arrows and recharge areas overlap the circuits and recharge area described by Tulipano et al. [41]; Figure S4. Simulated calcite Saturation Indexes (SI). Comparison between pure mixing (continuous line) and coupled model mixing+ion exchange (dashed lines) at different exchanger concentrations. Black dots indicate the calcite SI for the sampled waters (mixing > 3%); Figure S5. Carbonate mineral Saturation Indexes for the 47 groundwater samples; Table S1. Constructive features of monitoring wells. In italic and underscore are indicated MWs not equipped with in-place pumps; Table S2. Analytical methods applied for anions, cations, trace elements and dissolved organic carbon analysis and relative detection limits; Table S3. In the table are indicated the main statistics of measured parameters discussed in the paper; Table S4. In the table are indicated MWs, chloride concentration, the groundwater (GW) group based on chloride concentration, mixing percentage (f<sub>sea</sub>%), the  $\text{Na}/\text{Cl}$ ,  $\text{Cl}/\text{HCO}_3$  and  $\text{Ca}/\text{HCO}_3$  ratios and the cluster groups. In italic and underscore are indicated MWs not equipped with in-place pumps. The limits of GW groups are: (1)  $\text{Cl}^- < 250 \text{ mg/L}$ ; (2)  $250 \leq \text{Cl}^- < 700 \text{ mg/L}$ ; (3)  $700 \text{ mg/L} \leq \text{Cl}^- < 3000 \text{ mg/L}$ ; (4)  $\text{Cl}^- \geq 3000 \text{ mg/L}$ .  $\text{Na}/\text{Cl} < 0.90$  indicates MWs affected by SWI.  $\text{Cl}/\text{HCO}_3 < 0.5$  indicates MWs no affected by SWI;  $0.5 < \text{Cl}/\text{HCO}_3 < 1.3$  indicates MWs slightly affected by SWI;  $1.3 < \text{Cl}/\text{HCO}_3 < 2.8$  indicates MWs moderately affected by SWI;  $2.8 < \text{Cl}/\text{HCO}_3 < 6.6$  indicates MWs injuriously affected by SWI and  $\text{Cl}/\text{HCO}_3 > 6.6$  indicates MWs highly affected by SWI.  $\text{Ca}/\text{HCO}_3$  around 1 is typical of carbonate dissolution, around 0.5 is typical of dolomite dissolution and  $>1$  can be attributed to mixing with seawater and possible reverse ion exchange processes.

**Author Contributions:** Conceptualization, E.F., D.P., S.G., R.M., G.P. and E.P.; Methodology, E.F., D.P., S.G., R.M., G.P. and E.P.; Validation, D.P., S.G., M.S. and M.P.; Formal analysis, E.F. and D.P.;

Investigation, E.F., D.P., S.G., R.M. and G.P.; Data curation, E.F., D.P. and S.G.; Writing—original draft preparation, E.F. and D.P.; Writing—review and editing, E.F., D.P., S.G., R.M., G.P., M.S., M.P. and E.P.; Visualization, E.F. and D.P.; Supervision, G.P. and E.P.; Funding acquisition, R.M. and G.P. All authors have read and agreed to the published version of the manuscript.

**Funding:** This research was developed as an outcome of the research Project VIOLA on the assessment of natural background levels in the groundwater bodies of the Apulia region jointly developed with the Department of Water Resources Management of the Apulia Region funded by the Regional Department of Water Resources Management of the Apulia Region, within the frame of the Regional Operational Program (ROP) E.R.D.F.-E.S.F. 2014/2020.

**Institutional Review Board Statement:** Not applicable.

**Informed Consent Statement:** Not applicable.

**Data Availability Statement:** The data presented in this study are available on request from the corresponding author. The data are not publicly available due to privacy.

**Acknowledgments:** We wish to thank Marco Melita and Bepi Ferrari for their support during the sampling phase and Francesca Falconi and Domenico Mastroianni for chemical analyses.

**Conflicts of Interest:** The authors declare no conflict of interest.

## References

1. Vallejos, A.; Daniele, L.; Sola, F.; Molina, L.; Pulido-Bosch, A. Anthropogenic-induced salinization in a dolomite coastal aquifer. Hydrogeochemical processes. *J. Geochem. Explor.* **2020**, *209*, 106438. [\[CrossRef\]](#)
2. Alfarrach, N.; Walraevens, K. Groundwater overexploitation and seawater intrusion in coastal areas of arid and semi-arid regions. *Water* **2018**, *10*, 143. [\[CrossRef\]](#)
3. Mastrocicco, M.; Colombani, N. The issue of groundwater salinization in coastal areas of the mediterranean region: A review. *Water* **2021**, *13*, 90. [\[CrossRef\]](#)
4. Passarella, G.; Barca, E.; Sollitto, D.; Masciale, R.; Bruno, D.E. Cross-calibration of two independent groundwater balance models and evaluation of unknown terms: The case of the shallow aquifer of “Tavoliere di Puglia” (South Italy). *Water Resour. Manag.* **2017**, *31*, 327–340. [\[CrossRef\]](#)
5. Werner, A.D.; Bakker, M.; Post, V.E.A.; Vandenbohede, A.; Lu, C.; Ataie-Ashtiani, B.; Simmons, C.T.; Barry, D.A. Seawater intrusion processes, investigation and management: Recent advances and future challenges. *Adv. Water Resour.* **2013**, *51*, 3–26. [\[CrossRef\]](#)
6. Etsias, G.; Hamill, G.A.; Thomson, C.; Kennerley, S.; Águila, J.F.; Benner, E.M.; McDonnell, M.C.; Ahmed, A.A.; Flynn, R. Laboratory and numerical study of saltwater upconing in fractured coastal aquifers. *Water* **2021**, *13*, 3331. [\[CrossRef\]](#)
7. Pacheco-Castro, R.; Salles, P.; Canul-Macario, C.; Paladio-Hernandez, A. On the understanding of the hydrodynamics and the causes of saltwater intrusion on lagoon tidal springs. *Water* **2021**, *13*, 3431. [\[CrossRef\]](#)
8. Tulipano, L.; Fidelibus, D.; Panagopoulos, A. *Groundwater Management of Coastal Karstic Aquifers*; EU Publications Office: Luxembourg, 2005; ISBN 9289800151.
9. Telahigue, F.; Mejri, H.; Mansouri, B.; Souid, F.; Agoubi, B.; Chahlaoui, A.; Kharroubi, A. Assessing seawater intrusion in arid and semi-arid Mediterranean coastal aquifers using geochemical approaches. *Phys. Chem. Earth* **2020**, *115*, 102811. [\[CrossRef\]](#)
10. Rachid, G.; Alameddine, I.; El-Fadel, M. SWOT risk analysis towards sustainable aquifer management along the Eastern Mediterranean. *J. Environ. Manag.* **2021**, *279*, 111760. [\[CrossRef\]](#)
11. Kura, N.U.; Ramli, M.F.; Ibrahim, S.; Sulaiman, W.N.A.; Zaudi, M.A.; Aris, A.Z. A preliminary appraisal of the effect of pumping on seawater intrusion and upconing in a small tropical island using 2D resistivity technique. *Sci. World J.* **2014**, *2014*, 796425. [\[CrossRef\]](#)
12. Priyantha Ranjan, S.; Kazama, S.; Sawamoto, M. Effects of climate and land use changes on groundwater resources in coastal aquifers. *J. Environ. Manag.* **2006**, *80*, 25–35. [\[CrossRef\]](#) [\[PubMed\]](#)
13. Alexakis, D.; Tsakiris, G. Drought impacts on karstic spring annual water potential. Application on Almyros (Crete) brackish spring. *Desalin. Water Treat.* **2010**, *16*, 229–237. [\[CrossRef\]](#)
14. Cotecchia, V.; Lattanzio, M.; Polemio, M. Metodologie di studio e difesa dall'inquinamento salino degli acquiferi. In Proceedings of the VI Workshop del Progetto Strategico “Clima, Ambiente e Territorio nel Mezzogiorno”, Taormina, Italy, 13–15 December 1993; Volume I, pp. 417–446.
15. Ling, Z.; Shu, L.; Sun, Y.; Wang, R.; Li, Y. Impact of island urbanization on freshwater lenses: A case study on a small coral island. *Water* **2021**, *13*, 3272. [\[CrossRef\]](#)
16. Abdelkader, R.; Larbi, D.; Rihab, H.; Fethi, B.; Chemseddine, F.; Azzedine, H. Geochemical characterization of groundwater from shallow aquifer surrounding fetzara lake n. e. algeria. *Arab. J. Geosci.* **2012**, *5*, 1–13. [\[CrossRef\]](#)

17. Hermides, D.; Stamatis, G. Origin of halogens and their use as environmental tracers in aquifers of Thriassion Plain, Attica, Greece. *Environ. Earth Sci.* **2017**, *76*, 306. [[CrossRef](#)]
18. Lebid, H.; Errih, M.; Boudjemline, D. Contribution of strontium to the study of groundwater salinity. Case of the alluvial plain of Sidi Bel Abbes (Northwestern Algeria). *Environ. Earth Sci.* **2016**, *75*, 947. [[CrossRef](#)]
19. Sanchez Martos, F.; Bosch, A.P.; Calaforra, J.M. Hydrogeochemical processes in an arid region of Europe (Almeria, SE Spain). *Appl. Geochem.* **1999**, *14*, 735–745. [[CrossRef](#)]
20. Mirzavand, M.; Ghasemieh, H.; Sadatinejad, S.J.; Bagheri, R. An overview on source, mechanism and investigation approaches in groundwater salinization studies. *Int. J. Environ. Sci. Technol.* **2020**, *17*, 2463–2476. [[CrossRef](#)]
21. Cao, T.; Han, D.; Song, X. Past, present, and future of global seawater intrusion research: A bibliometric analysis. *J. Hydrol.* **2021**, *603*, 126844. [[CrossRef](#)]
22. Zaccaria, D.; Passarella, G.; D’Agostino, D.; Giordano, R.; Solis, S.S. Risk assessment of aquifer salinization in a large-scale coastal irrigation scheme, Italy. *Clean—Soil Air Water* **2016**, *44*, 371–382. [[CrossRef](#)]
23. Capaccioni, B.; Didero, M.; Paletta, C.; Didero, L. Saline intrusion and refreshing in a multilayer coastal aquifer in the Catania Plain (Sicily, Southern Italy): Dynamics of degradation processes according to the hydrochemical characteristics of groundwaters. *J. Hydrol.* **2005**, *307*, 1–16. [[CrossRef](#)]
24. Abu-alnaeem, M.F.; Yusoff, I.; Ng, T.F.; Alias, Y.; Raksmei, M. Assessment of groundwater salinity and quality in Gaza coastal aquifer, Gaza Strip, Palestine: An integrated statistical, geostatistical and hydrogeochemical approaches study. *Sci. Total Environ.* **2018**, *615*, 972–989. [[CrossRef](#)] [[PubMed](#)]
25. Tiwari, A.K.; Pisciotta, A.; De Maio, M. Evaluation of groundwater salinization and pollution level on Favignana Island, Italy. *Environ. Pollut.* **2019**, *249*, 969–981. [[CrossRef](#)]
26. Kazakis, N.; Busico, G.; Colombani, N.; Mastrocicco, M.; Pavlou, A.; Voudouris, K. GALDIT-SUSI a modified method to account for surface water bodies in the assessment of aquifer vulnerability to seawater intrusion. *J. Environ. Manag.* **2019**, *235*, 257–265. [[CrossRef](#)]
27. Chucuya, S.; Vera, A.; Pino-Vargas, E.; Steenken, A.; Mahlknecht, J.; Montalván, I. Hydrogeochemical characterization and identification of factors influencing groundwater quality in coastal aquifers, case: La Yarada, Tacna, Peru. *Int. J. Environ. Res. Public Health* **2022**, *19*, 2815. [[CrossRef](#)] [[PubMed](#)]
28. Boumaiza, L.; Chesnaux, R.; Drias, T.; Walter, J.; Huneau, F.; Garel, E.; Knoeller, K.; Stumpp, C. Identifying groundwater degradation sources in a Mediterranean coastal area experiencing significant multi-origin stresses. *Sci. Total Environ.* **2020**, *746*, 141203. [[CrossRef](#)] [[PubMed](#)]
29. Ben Hamouda, M.F.; Tarhouni, J.; Leduc, C.; Zouari, K. Understanding the origin of salinization of the Plio-quadernary eastern coastal aquifer of Cap Bon (Tunisia) using geochemical and isotope investigations. *Environ. Earth Sci.* **2011**, *63*, 889–901. [[CrossRef](#)]
30. Abou Zakhem, B.; Hafez, R. Environmental isotope study of seawater intrusion in the coastal aquifer (Syria). *Environ. Geol.* **2007**, *51*, 1329–1339. [[CrossRef](#)]
31. Argamasilla, M.; Barberá, J.A.; Andreo, B. Factors controlling groundwater salinization and hydrogeochemical processes in coastal aquifers from southern Spain. *Sci. Total Environ.* **2017**, *580*, 50–68. [[CrossRef](#)]
32. Giménez-Forcada, E.; Vega-Alegre, M. Arsenic, barium, strontium and uranium geochemistry and their utility as tracers to characterize groundwaters from the Espadán-Calderona Triassic Domain, Spain. *Sci. Total Environ.* **2015**, *512–513*, 599–612. [[CrossRef](#)]
33. Petalas, C.P. A preliminary assessment of hydrogeological features and selected anthropogenic impacts on an alluvial fan aquifer system in Greece. *Environ. Earth Sci.* **2013**, *70*, 439–452. [[CrossRef](#)]
34. Han, D.; Post, V.E.A.; Song, X. Groundwater salinization processes and reversibility of seawater intrusion in coastal carbonate aquifers. *J. Hydrol.* **2015**, *531*, 1067–1080. [[CrossRef](#)]
35. Souid, F.; Agoubi, B.; Telahigue, F.; Chahlaoui, A.; Kharroubi, A. Groundwater salinization and seawater intrusion tracing based on Lithium concentration in the shallow aquifer of Jerba Island, southeastern Tunisia. *J. Afr. Earth Sci.* **2018**, *138*, 233–246. [[CrossRef](#)]
36. Canora, F.; Fidelibus, M.D.; Sciortino, A.; Spilotro, G. Variation of infiltration rate through karstic surfaces due to land use changes: A case study in Murgia (SE-Italy). *Eng. Geol.* **2008**, *99*, 210–227. [[CrossRef](#)]
37. Barbieri, M.; Barbieri, M.; Fidelibus, D.; Morotti, M.; Sappa, G.; Tulipano, L. First results of the application of the isotopic ratio  $^{87}\text{Sr}/^{86}\text{Sr}$  in the characterization of sea-water intrusion in the coastal karstic aquifer of Murgia (Southern Italy). *Natuurwet. Tijdschr.* **1999**, *79*, 132–139.
38. Ciaranfi, N.; Pieri, P.; Ricchetti, G. Note alla carta geologica delle Murge e del Salento (*Puglia centromeridionale*). *Mem. Soc. Geol. Ital.* **1988**, *41*, 449–460.
39. Cotecchia, V.; Grassi, D.; Polemio, M. Carbonate aquifers in Apulia and seawater intrusion. *G. Geol. Appl.* **2005**, *1*, 219–231. [[CrossRef](#)]
40. Masciale, R.; Amalfitano, S.; Frollini, E.; Ghergo, S.; Melita, M.; Parrone, D.; Preziosi, E.; Vurro, M.; Zoppini, A.; Passarella, G. Assessing natural background levels in the groundwater bodies of the Apulia region (Southern Italy). *Water* **2021**, *13*, 958. [[CrossRef](#)]

41. Tulipano, L.; Cotecchia, V.; Fidelibus, M.D. An example of the multitracing approach in studies of karstic and coastal aquifers. In *Hydrogeological Processes in Karst Terranes, Proceedings of the International Symposium and Field Seminar, Antalya, Turkey, 7–17 October 1990*; International Association of Hydrological Sciences: Wallingford, UK, 1993; pp. 381–389.
42. Kottek, M.; Grieser, J.; Beck, C.; Rudolf, B.; Rubel, F. World map of the Köppen-Geiger climate classification updated. *Meteorol. Z.* **2006**, *15*, 259–263. [[CrossRef](#)]
43. Passarella, G.; Bruno, D.; Lay-Ekuakille, A.; Maggi, S.; Masciale, R.; Zaccaria, D. Spatial and temporal classification of coastal regions using bioclimatic indices in a Mediterranean environment. *Sci. Total Environ.* **2020**, *700*, 134415. [[CrossRef](#)]
44. Maggi, S.; Bruno, D.; Lay-Ekuakille, A.; Masciale, R.; Passarella, G. Automatic processing of bioclimatic data in the space and time domains. *J. Phys. Conf. Ser.* **2018**, *1065*, 192005. [[CrossRef](#)]
45. Frollini, E.; Rossi, D.; Rainaldi, M.; Parrone, D.; Ghergo, S.; Preziosi, E. A proposal for groundwater sampling guidelines: Application to a case study in southern Latium. *Rend. Online Soc. Geol.* **2019**, *47*, 46–51. [[CrossRef](#)]
46. Appelo, C.A.J.; Postma, D. *Geochemistry, Groundwater and Pollution*, 2nd ed.; A.A. Balkema Publishers: Leiden, The Netherlands, 2005; ISBN 9054101059.
47. Hammer, D.A.T.; Ryan, P.D.; Hammer, Ø.; Harper, D.A.T. Past: Paleontological statistics software package for education and data analysis. *Palaeontol. Electron.* **2001**, *4*, 9.
48. Jiao, J.; Post, V. *Coastal Hydrogeology*; Cambridge University Press: Cambridge, UK, 2019; ISBN 9781139344142.
49. Lee, S.; Currell, M.; Cendón, D.I. Marine water from mid-Holocene sea level highstand trapped in a coastal aquifer: Evidence from groundwater isotopes, and environmental significance. *Sci. Total Environ.* **2016**, *544*, 995–1007. [[CrossRef](#)]
50. Sit.Puglia. Available online: [http://www.sit.puglia.it/portal/portale\\_cis/CorpiIdriciSotterranei/DatidelMonitoraggio](http://www.sit.puglia.it/portal/portale_cis/CorpiIdriciSotterranei/DatidelMonitoraggio) (accessed on 29 April 2022).
51. Parkhurst, D.L.; Appelo, C.A.J. Description of input and examples for PHREEQC version 3—A computer program for speciation, batch-reaction, one-dimensional transport, and inverse geochemical calculations. U.S. Geological Survey techniques and methods. In *Book 6, Modeling Techniques*; U.S. Geological Survey: Denver, CO, USA, 2013; p. 497. ISBN 0092-332X.
52. Yechieli, Y.; Kafri, U.; Sivan, O. The inter-relationship between coastal sub-aquifers and the Mediterranean Sea, deduced from radioactive isotopes analysis. *Hydrogeol. J.* **2009**, *17*, 265–274. [[CrossRef](#)]
53. Tropeano, M.; Sabato, L.; Pieri, P. The Quaternary post-turbidite sedimentation in the south-Appennines foredeep (Bradanic Trough-southern Italy). *Boll. Soc. Geol. Ital.* **2002**, *121*, 449–454.
54. Lee, J.Y.; Song, S.H. Evaluation of groundwater quality in coastal areas: Implications for sustainable agriculture. *Environ. Geol.* **2007**, *52*, 1231–1242. [[CrossRef](#)]
55. El Moujabber, M.; Bou Samra, B.; Darwish, T.; Atallah, T. Comparison of different indicators for groundwater contamination by seawater intrusion on the Lebanese coast. *Water Resour. Manag.* **2006**, *20*, 161–180. [[CrossRef](#)]
56. Mtoni, Y.; Mjemah, I.C.; Bakundukize, C.; Van Camp, M.; Martens, K.; Walraevens, K. Saltwater intrusion and nitrate pollution in the coastal aquifer of Dar es Salaam, Tanzania. *Environ. Earth Sci.* **2013**, *70*, 1091–1111. [[CrossRef](#)]
57. Salvadori, M.; Frollini, E.; Ghergo, S.; Masciale, R.; Parrone, D.; Passarella, G.; Preziosi, E.; Pennisi, M. Interpreting salinization phenomena in the coastal groundwater of the Murgia aquifer (Apulia, Southern Italy) by means of B, Sr, O, and H isotopes. In *Proceedings of the IAH 2021 Congress, Brussels, Belgium, 6–10 September 2021*; p. 281.
58. Hodell, D.A.; Mead, G.A.; Mueller, P.A. Variation in the strontium isotopic composition of seawater (8 Ma to present): Implications for chemical weathering rates and dissolved fluxes to the oceans. *Chem. Geol. Isot. Geosci. Sect.* **1990**, *80*, 291–307. [[CrossRef](#)]
59. Frijia, G.; Parente, M.; Di Lucia, M.; Mutti, M. Carbon and strontium isotope stratigraphy of the Upper Cretaceous (Cenomanian-Campanian) shallow-water carbonates of southern Italy: Chronostratigraphic calibration of larger foraminifera biostratigraphy. *Cretac. Res.* **2015**, *53*, 110–139. [[CrossRef](#)]
60. Angino, E.E.; Billings, G.K.; Andersen, N. Observed variations in the strontium concentration of sea water. *Chem. Geol.* **1966**, *1*, 145–153. [[CrossRef](#)]
61. Fidelibus, M.D.; Calò, G.; Tinelli, R.; Tulipano, L. Salt ground waters in the Salento karstic coastal aquifer (Apulia, Southern Italy). In *Advances in the Research of Aquatic Environment*; Springer: Berlin/Heidelberg, Germany, 2011; pp. 407–415. ISBN 9783642199028.
62. Appelo, C.A.J.; Willemssen, A. Geochemical calculations and observations on salt water intrusions, I. A combined geochemical/minxing cell model. *J. Hydrol.* **1987**, *94*, 313–330. [[CrossRef](#)]
63. Appelo, C.A.J. Cation and proton exchange, pH variations, and carbonate reactions in a freshening aquifer. *Water Resour. Res.* **1994**, *30*, 2793–2805. [[CrossRef](#)]
64. Ball, J.W.; Nordstrom, D.K. *User's Manual for WATEQ4F, with Revised Thermodynamic Data Base and Text Cases for Calculating Speciation of Major, Trace, and Redox Elements in Natural Waters*; Version 2; U.S. Department of Interior: Menlo Park, CA, USA, 1991.
65. Freeze, R.A.; Cherry, J.A. *Groundwater*; Prentice Hall: Hoboken, NJ, USA, 1979; ISBN 0133653129.